FERROELECTRICITY

Metal-free three-dimensional perovskite ferroelectrics

Heng-Yun Ye[1]*†, Yuan-Yuan Tang[1]*, Peng-Fei Li[1]*, Wei-Qiang Liao[1,2], Ji-Xing Gao[1], Xiu-Ni Hua[1], Hu Cai[2], Ping-Ping Shi[1,3], Yu-Meng You[1]‡, Ren-Gen Xiong[1,2]‡

Inorganic perovskite ferroelectrics are widely used in nonvolatile memory elements, capacitors, and sensors because of their excellent ferroelectric and other properties. Organic ferroelectrics are desirable for their mechanical flexibility, low weight, environmentally friendly processing, and low processing temperatures. Although almost a century has passed since the first ferroelectric, Rochelle salt, was discovered, examples of highly desirable organic perovskite ferroelectrics are lacking. We found a family of metal-free organic perovskite ferroelectrics with the characteristic three-dimensional structure, among which MDABCO (*N*-methyl-*N*′-diazabicyclo[2.2.2]octonium)–ammonium triiodide has a spontaneous polarization of 22 microcoulombs per square centimeter [close to that of barium titanate (BTO)], a high phase transition temperature of 448 kelvins (above that of BTO), and eight possible polarization directions. These attributes make it attractive for use in flexible devices, soft robotics, biomedical devices, and other applications.

The word "perovskite" is derived from the mineral $CaTiO_3$, which was first discovered by Gustav Rose in 1839 (*1*). Magnesium silicate perovskite and calcium silicate perovskite are also the most abundant minerals in Earth's interior (*2*). Typical perovskites have a distinct three-dimensional (3D) ABX_3 crystal structure, in which the A cations are located in the 3D corner-sharing framework of BX_6 octahedrons (B represents the other cation and X is an anion) (*3*). There are hundreds of known perovskites, constituting an essential class of functional materials in optoelectronics and microelectronics. Among their numerous attractive properties, ferroelectricity, which is the ability to switch spontaneous polarization (P_s) under an applied electric field, is of particular interest for theoretical studies and is important for a variety of applications (*4*–*7*).

Inorganic perovskites, such as $BaTiO_3$ (BTO) and $Pb(Zr,Ti)O_3$, dominate applications such as ferroelectric memories, piezoelectric sensors, actuators, capacitors, and nonlinear optical devices (*8*–*10*). However, the requirements for practical materials to be energy efficient, economically inexpensive, and environmentally friendly ("triple E") motivate the exploration for nontoxic, low-cost, and simple alternatives to inorganic perovskites (*11*). Organic compounds in general and hybrid organic-inorganic perovskites in particular are attractive alternatives. These materials are lightweight, low cost, mechanically flexible, structurally tunable, and easy to process. These properties make organics attractive for materials science and technology applications (*12*, *13*).

Several different hybrid halide organic-inorganic perovskites have notable properties. Hybrid halide perovskites such as $(CH_3NH_3)PbI_3$ and $(CH_3NH_3)PbBr_3$ have attracted much attention in the solar cell and light-emitting diode (LED) fields because of their outstanding photovoltaic and luminescent performance (*14*–*19*). A few organic-inorganic perovskite ferroelectrics containing halides, cyanides, and formates were developed as competitive candidates for microelectromechanical systems (MEMS) (*20*–*25*). We recently synthesized trimethylchloromethyl ammonium trichloromanganese(II), which has a large piezoelectric response and displays ferroelectric properties comparable to those of BTO (*13*).

An underexplored but intriguing area for developing ferroelectric materials is metal-free, or organic, perovskites. These materials have an organic cation occupying the B site of the crystal. The organic composition should allow for wide chemical diversity, structural flexibility, and additional functionalities that are difficult to achieve with inorganic perovskites. The concerns with organic perovskites are that the absence of the metal ion will affect the stability of the 3D perovskites and they may not be good ferroelectric materials. In 2002, a molecular perovskite hydrate, $(C_4H_{12}N_2)(NH_4Cl_3)\cdot H_2O$, featuring the piperazinium cation $(C_4H_{12}N_2)^{2+}$ and water molecules enclosing the 3D corner-sharing $[(NH_4)Cl_6]$ network, was described (*26*). The discovery marked the beginning for metal-free perovskites, although this perovskite has an ABX_3C rather than a real ABX_3 structure (*26*, *27*). Such a system is promising for constructing noncentrosymmetric or polar structures and homochiral analogs. However, 15 years after the initial discovery of metal-free perovskites, no observations of ferroelectricity or other functionalities have been reported.

We used a molecular design strategy (see supplementary materials) (*28*) and elaborate selection of the organic cations to develop a family of metal-free ABX_3-type 3D perovskite ferroelectrics, with the general formula of $A(NH_4)X_3$ (where A is a divalent organic cation and X is Cl, Br, or I, as listed in Fig. 1A). We synthesized a total of 23 different members of this family with a range of different structures (tables S1 to S9) and phase transition temperatures (table S10). Among the first $A(NH_4)X_3$ perovskites we discovered, MDABCO–NH_4I_3 (MDABCO is *N*-methyl-*N*′-diazabicyclo[2.2.2]octonium) has a high phase transition temperature (T_0) of 448 K and a large P_s of 22 $\mu C/cm^2$, which are comparable to those of BTO (table S11). Furthermore, using piezoresponse force microscopy (PFM), we discovered the coexistence of various ferroelectric domains with eight polarization directions and evidence for the flexible rotation of polarization directions by the application of an electric field. Our strategy demonstrates the viability of high-performance metal-free ferroelectric perovskites. Without the metal element, such organics are expected to be on par with their inorganic and organic-inorganic counterparts, enhanced by the high flexibility, tunable structure-property relationships, possible solution and vacuum processes, and biocompatibility of organic materials.

General structures

Our metal-free 3D perovskite ferroelectrics are all the classical ABX_3 type without water, with 3D networks of corner-shared $(NH_4)X_6$ (X is Cl, Br, or I) octahedra that enclose cavities occupied by the divalent organic ammonium cations, and all components are held together by ionic and hydrogen-bonding interactions (Fig. 1 and figs. S1 to S18). We collected x-ray diffraction data and determined the crystal data for the structures (tables S4 to S9). Most of these metal-free perovskite structures crystallize in the ferroelectric space group at room temperature. We summarize the space groups of their ferroelectric and paraelectric phases and the Curie temperatures in table S10.

We evaluated ionic size mismatches in this large class of metal-free perovskite compounds by calculating the geometrical parameter $\alpha = (R_A + R_X)/\sqrt{2}(R_B + R_X)$. This is the tolerance factor introduced by V. M. Goldschmidt in 1926 (*29*). According to the definition, R_i is the radii of the ions in the perovskite ABX_3, where i is A, B, and X, respectively. We obtained the radii of R_A from experimental single-crystal x-ray diffraction. All of the tolerance factors for the presented divalent cations in the NH_4X_3 cavities range between 0.87 and 1.00 (fig. S19 and table S12). For values of α in the range of 0.9 to 1.0, we found 3D perovskites with greater probability, consistent with the previous analysis (*30*). Values of 0.87 to 0.89 lead to 1D hexagonal structures. A stable 3D perovskite structure does not depend solely

[1]Jiangsu Key Laboratory for Science and Applications of Molecular Ferroelectrics, Southeast University, Nanjing 211189, P.R. China. [2]Ordered Matter Science Research Center, Nanchang University, Nanchang 330031, P.R. China. [3]Institute for Advanced Interdisciplinary Research, Nanjing University of Aeronautics and Astronautics, Nanjing 211106, P.R. China.
*These authors contributed equally to this work. †Present address: Chaotic Matter Science Research Center, Jiangxi University of Science and Technology, Ganzhou, 341000, P.R. China.
‡Corresponding author. Email: youyumeng@seu.edu.cn (Y.-M.Y.); xiongrg@seu.edu.cn (R.-G.X.)

on ionic size mismatching. It also requires intermolecular interactions, such as van der Waals forces and hydrogen bonding, to become predominant in the pure organic perovskite materials. The 3D perovskite structure of DABCO–NH_4Br_3 (DABCO is *N*-*N*′-diazabicyclo[2.2.2]octonium) with α = 0.88 is a good demonstration of the comprehensive and sophisticated factors involved in the stable formation of the 3D perovskite structure.

MDABCO–NH_4I_3

Ferroelectric phase

MDABCO–NH_4I_3 has a relatively simple 3D structure (a unit cell contains just one molecular unit) (fig. S1), and thus we take it here as an example to elucidate the ferroelectric mechanism. At room temperature, MDABCO–NH_4I_3 crystallizes in the polar space group *R*3, *Z* = 1 (where Z is the number of formula units), with unit cell dimensions $a = b = c = 7.259(4)$ Å and $\alpha = \beta = \gamma = 84.767(4)°$ (where numbers in parentheses indicate uncertainty). In the cage-like unit cell, the MDABCO cation locates at the center, NH_4^+ groups locate at vertexes, and I^- ions are at the centers of the edges. According to the Curie symmetry superposition principle, the symmetry group of the specific assembly mode of the MDABCO–NH_4I_3 crystal adopts the maximal common subgroup of its composition molecular symmetry groups. In the crystal of MDABCO–NH_4I_3, $MDABCO^{2+}$ and NH_4^+ are arranged alternately along the crystallographic [1 1 1] direction (Fig. 1B), and both the intramolecular C_3 axes of these two molecules are superimposed with the crystallographic C_3 axis. As the symmetry groups of the $MDABCO^{2+}$ and NH_4^+ molecules are C_3 and T_d, respectively, the maximal common subgroup will be the C_3 point group. During the molecular assembly, the symmetry elements of $\bar{4}$ and *m* from point group T_d disappear, and both symmetry elements of 3 from point groups T_d and C_3 are preserved. The resultant polar point group symmetry C_3 should lead to the generation of spontaneous polarization along the [1 1 1] direction, because the $MDABCO^{2+}$ molecule carries a dipole moment along the molecular threefold axis. The polar point group in such metal-free frameworks is not expected when we replace $MDABCO^{2+}$ with $DABCO^{2+}$, because of the D_{3h} symmetry of $DABCO^{2+}$. While in the paraelectric phase, the disordered $MDABCO^{2+}$ molecule can be regarded as a special spherical configuration with *O* point group symmetry composed of all eight orientations possible in the ferroelectric phase. Such dynamically disordered behavior of the $MDABCO^{2+}$ molecule is responsible for the 432 symmetry of its paraelectric phase.

Paraelectric phase

At T_0 = 448 K, MDABCO–NH_4I_3 transforms into the cubic paraelectric phase, which features the space group *P*432, *a* = 7.516(13) Å, *Z* =1. In the paraelectric phase, MDABCO becomes disordered and the $(NH_4)I_6$ octahedron becomes regular (fig. S1B). MDABCO is located on the special site of 432 symmetry. The high-symmetry site of 432 requires total disorder of the organic cation, and accordingly, we modeled MDABCO with a spherical structure discarding its chemical sense (Fig. 1C). This suggests that the MDABCO cations are nearly freely rotating in the high-temperature paraelectric phase. Dynamic disorder of organic molecules in crystals is usually observed for those molecules with spherical geometries, such as tetramethylammonium, adamantane, and DABCO. Compared with that of DABCO, the shape of MDABCO deviates just slightly from the spherical geometry (Fig. 1B, blue oval). Such a molecular geometry is the key element for the generation of ferroelectricity. On the one hand, the quasispherical geometry makes molecular reorientation easy, which is necessary for ferroelectric polarization reversal (*9*). On the other hand, the lowering of molecular symmetry through the attachment of a methyl group to DABCO leads to the generation of dipole moments, whose alignment results in the symmetry breaking and contributes to the polarization of the crystal. According to the symmetry change, MDABCO–NH_4I_3 belongs to the ferroelectric species of 432*F*3 (*31*).

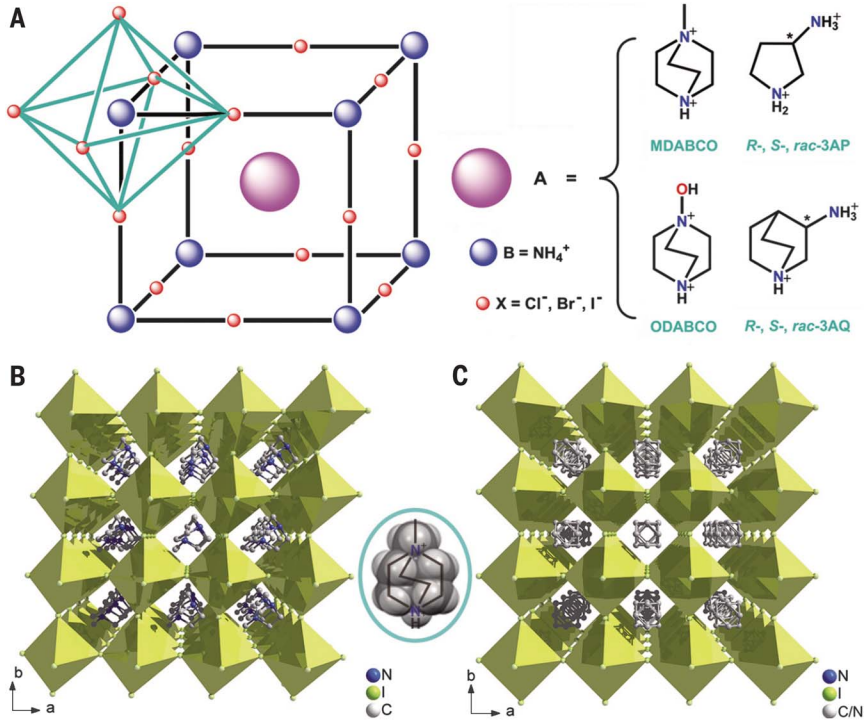

Fig. 1. Chemical and crystal structures of the metal-free $A(NH_4)X_3$ family. (**A**) Chemical structures of constituents of the metal-free 3D perovskite ferroelectrics. (**B**) The packing diagram of MDABCO–NH_4I_3 in the ferroelectric phase at 293 K. The oval to the right contains the space-fill diagram of the organic cation, showing the cationic geometry to be close to a ball. (**C**) The packing diagram of MDABCO–NH_4I_3 in the paraelectric phase at 463 K.

Because of the high symmetry of DABCO, the DABCO-containing molecular analogs, such as DABCO–$(NH_4)Br_3$ (fig. S13) and DABCO–$RbCl_3$ (*27*), do not have ferroelectricity. Additionally, the suitable size of the MDABCO ion allows it to template the 3D perovskite structure. Meanwhile, we also isolated hexagonal organic perovskites DABCO–$(NH_4)X_3$ (where X is Cl or I) and found that these materials do not show spontaneous polarization (figs. S14 and S15).

General characterizations

A pair of reversible thermal anomalies in the differential scanning calorimetry (DSC) curves reveal a phase transition around 448 K for MDABCO–NH_4I_3 (Fig. 2A). This T_0 is higher than those of the vast majority of high-temperature molecular ferroelectrics and BTO (393 K). We estimated the entropy change (ΔS) accompanying the phase transition to be ~50 J mol^{-1} K^{-1}. The main contribution of the high ΔS should be from the transition of the MDABCO cation from a freely rotating state to a static state. Meanwhile, we also confirmed the phase transition by the temperature-dependent second-harmonic generation (SHG) response (fig. S20). The detectable SHG intensity vanishes for temperatures above T_0, supporting the notion of a phase transition from the polar 3 point group into a nonpolar 432 one, which should have null SHG response under the restriction of Kleinman symmetry (*32*).

The real part (ε′) of the complex dielectric constant ($\varepsilon = \varepsilon' - i\varepsilon''$, where *i* is the imaginary unit and ε″ is the imaginary part of ε) as a function of temperature at various frequencies shows a prominent λ-shape peak anomaly around T_0 along the [1 1 1] direction (Fig. 2B), indicative of a proper ferroelectric transition. The peak value increases with decreasing frequency and reaches

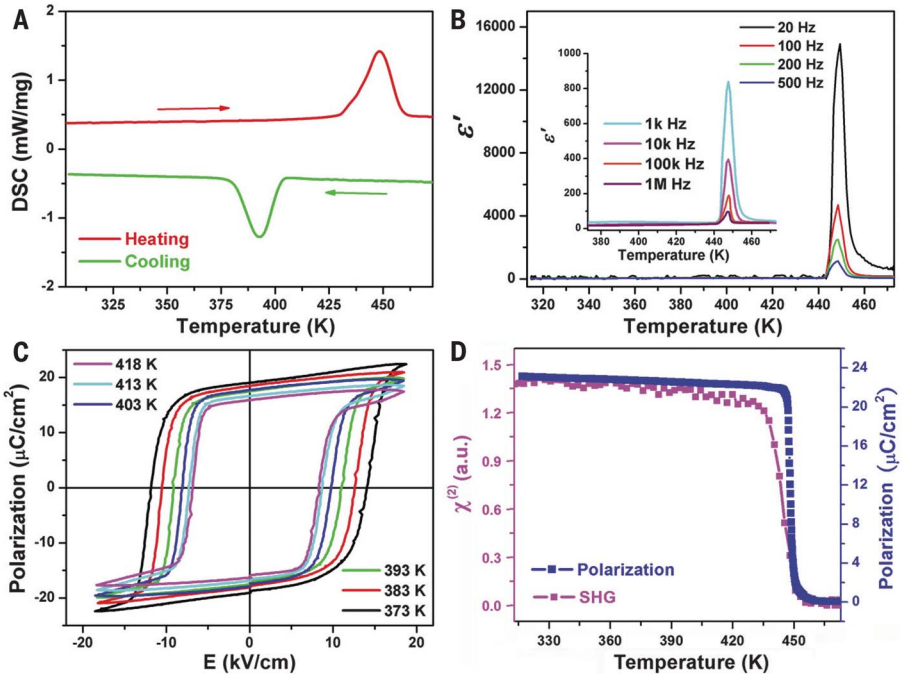

Fig. 2. Ferroelectric properties of MDABCO–NH_4I_3. (**A**) The results of DSC measurements, revealing a structural phase transition at around T_0 = 448 K. (**B**) The temperature dependence of the real part (ε′) of the complex dielectric constant at selected frequencies. k indicates thousands, and M represents a million. (**C**) *P-E* hysteresis loops measured at various temperatures. (**D**) Spontaneous polarization P_s and second-order nonlinear optical coefficient $\chi^{(2)}$ as a function of temperature. a.u., arbitrary units.

a large value of about 14,068 at 20 Hz. The dielectric response obeys the Curie-Weiss law well; that is, $\varepsilon = C/(T - T_c)$, where ε is the dielectric constant, C is the Curie constant, T ($T > T_c$) is the temperature, and T_c is the Curie-Weiss temperature. The reciprocal value of ε′ at 20 Hz as a function of temperature is linear, with the fitted Curie-Weiss constant C of 14,068 K, which is further evidence for a proper ferroelectric phase transition (fig. S21).

We used the Berlincourt method (*13*) to measure the piezoelectric coefficient d_{33} on the single crystal of MDABCO–NH_4I_3. At room temperature, we obtained a maximum d_{33} of ~14 pC/N along the [111] direction of the crystal (fig. S22). To investigate the optoelectronic potential, we also examined the optical absorption and emission properties by ultraviolet-visible absorption and photoluminescence spectroscopies, which showed that most of the perovskites tested are wide–band gap insulators and only those containing iodide can exhibit photoluminescence with the maximum emission wavelength of 561 nm (figs. S23 to 25).

Ferroelectricity

We further confirmed the ferroelectricity of MDABCO–NH_4I_3 by the measurement of polarization–electric field (*P-E*) hysteresis loops on the (1 1 1) plane recorded with the Sawyer-Tower circuit method (*33*) (Fig. 2C). We estimated the P_s value at 373 K as 19 μC/cm^2. The coercive field E_c is in the range of 6 to 12 kV/cm, comparable to that of BTO (10 kV/cm) and much smaller than that of polyvinylidene difluoride (PVDF) (500 kV/cm) (*34*). We also used pyroelectric measurements to evaluate the spontaneous polarization P_s. Spontaneous polarization appears below T_0 (Fig. 2D) and then gradually increases to a saturated value of 22 μC/cm^2, which is close to the values of 23 μC/cm^2 for diisopropylammonium bromide and 26 μC/cm^2 for BTO and greater than the 8 μC/cm^2 for PVDF and those for other organic-inorganic perovskite molecular ferroelectrics (*35*). The variation of P_s has the same trend as the effective second-order nonlinear optic susceptibility $\chi^{(2)}$, in good agreement with the Landau relationship $\chi^{(2)} = 6\varepsilon_0\beta P_s$, where β represents a coefficient almost independent of the temperature (*36*). The variations of both P_s and $\chi^{(2)}$ in the vicinity of T_0 are abrupt, revealing a typically first-order phase transition.

Spontaneous polarization

The mechanism of ferroelectric spontaneous polarization has different characteristics. Because of the ABX_3-type perovskite structure and metal-free composition, the origin of polarization in MDABCO–NH_4I_3 is more complicated than that in conventional inorganic perovskites, such as BTO, and organic-inorganic hybrid perovskites, such as $(CH_3NH_3)PbI_3$.

In the classic ABO_3-type inorganic perovskite, such as BTO, spontaneous polarization is induced by the off-centering displacement (OCD) of the small cation at the B site. Such phase transition is mainly displacive (*37*), with some contributions from order-disorder characteristics (*38*). Similar to the B-site cation in BTO, the B-site NH_4^+ ion in MDABCO–NH_4I_3 undergoes 0.2734-Å displacement from the center of the six surrounding I^- ions during the phase transition because of the octahedral tilting near T_0. The OCD of the B-site NH_4^+ ion is determined along the [111] direction. Besides OCD of the B-site NH_4^+ ion, the charge transfer through the N_{NH4}–H···I hydrogen bonds (where N_{NH4} indicates the N atom of NH_4^+ and ··· indicates interaction between H and I) should also contribute to the polarization. Those hydrogen-bonding interactions [$d_{H\cdots N}$ ($H_{NH4}\cdots N_{NH4}$ distance), 0.9 Å; $d_{H\cdots I}$ ($H_{NH4}\cdots I$ distance), 2.78 Å; ∠NHI, 159.7°; and $d_{N\cdots I}$, 3.637(9) Å] (fig. S26) are formed in the ferroelectric phase with the ordering of hydrogen bonds within the $(NH_4)I_6$ octahedron. Thus, for the B site, both charge transfer and OCD contribute to the ferroelectric polarization.

On the other hand, because of the metal-free composition and nature of molecular ferroelectrics, different from those of BTO, the A-site MDABCO also plays an important role in the generation of ferroelectricity. During the paraelectric-ferroelectric phase transition, A-site MDABCO changes from a nearly free rotation state to a static state. Such freezing of the dynamic motion tends to be discontinuous (*22*, *39*–*41*), and the ordering of the MDABCO cation leads not only to the alignment of the molecular dipole moment but also to substantial displacement. For conventional order-disorder–type inorganic compounds or organic salts, such as $NaNO_2$, KH_2PO_4, and triglycine sulfate (*9*, *10*), the order-disorder transitions are usually continuous and displacements of those dipoles are small and contribute a little spontaneous polarization accordingly. In MDABCO–NH_4I_3, the polarization direction induced by the displacement is the same as that of the molecular dipole moment of MDABCO (fig. S27). The displacement of ~0.65 Å is induced by the shift of the positive charge carried by MDABCO, which is accompanied by the elongation of the cubic cell along the body diagonal. In this sense, the ferroelectric contribution of the A site is essentially the displacive type.

The new class of metal-free perovskite ferroelectrics has a distinct polarization origin, different not only from that of conventional inorganic perovskites but also from that of organic-inorganic hybrid perovskites, such as $(CH_3NH_3)PbI_3$. The order-disorder mechanism has been found to dominate the phase transitions of those hybrid perovskites, such as $(CH_3NH_3)PbI_3$ (*42*, *43*) and $[(CH_3)_2NH_2]M(HCOO)_3$ (M is Zn, Mn, Fe, Co, or Ni) (*23*, *24*). In those organic-inorganic hybrid perovskites, the hydrogen-bonding interactions between the A-site organic ammoniums and the X-site anions play an important role. The order-disorder transitions are accompanied by the formation and breaking of hydrogen bonds. On the contrary, in MDABCO–NH_4I_3, the possible hydrogen bonding between the A-site MDABCO and the X-site I^- ion is through the N_{MDABCO}–H···I interactions, which are not suitable to form a

classic hydrogen bond because the distance of $d_{H\cdots A}$ is too large [$d_{H\cdots I}$ = 3.2098(10) Å] (*44*). Nevertheless, the weak N_{MDABCO}–H···I interactions also contribute to the spontaneous polarization (fig. S27). Because other atoms are farther away from I^- ions, the A-site MDABCO should be stabilized mostly by the ionic interactions, as supported by the density functional theory (DFT) calculations (figs. S28 to S30). The relatively low coercive electric field (E_c) may be related to the lack of strong hydrogen-bonding interactions, along with the quasispherical molecular geometry and the relatively large cavity enclosed by the octahedra.

At this stage, one can conclude that the ferroelectricity in MDABCO–NH_4I_3 is mainly ionic and influenced by hydrogen-bonding effects and that the large spontaneous polarization probably results from the parallel contributions of the displacement of charges, the alignment of the molecular dipole moments, hydrogen bond effects, and electronic contributions.

PFM characterization

Finally, we used PFM to observe the polarization ordering and switching dynamics of MDABCO–NH_4I_3 (*45*–*48*). Initial testing of single crystals (along the [1 1 1] direction) (figs. S31 and S32) indicates that the organic perovskite is dominated mainly by a large-area single-domain state with out-of-plane polarization (fig. S33). We were able to generate box-in-box bipolar domain patterns after applying a tip bias of +100 V in a 10 μm by 10 μm area and then −100 V in a centered 5 μm by 5 μm square region, demonstrating that the polarization of the ferroelectric domain can be switched back and forth in the MDABCO–NH_4I_3 crystal (Fig. 3A). In the microcrystalline state of the material, because of the existence of stress imposed by the matrix, non-180° domains with different polarization directions can appear. These twin domains can form various patterns, including stripes, which is typical for materials such as $BiFeO_3$ (Fig. 3B and fig. S34) and occurs sometimes when multiple domains intersect one another (Fig. 3C). To identify different polarization directions and analyze the angles between them, we performed comprehensive PFM studies for patterns with multiple domain intersections (figs. S35 to S38), the results of which clearly indicate the existence of eight polarization directions, corresponding well with the four polar axes deduced from the 432*F*3 transition. Most notably, we also successfully realized the rotation of the polarization direction in the MDABCO–NH_4I_3 microcrystal by using an external electric field, as the out-of-plane amplitude intensities of the central zone change from weak to strong in Fig. 3D. The emerging domain shape tends toward a hexagon, in good agreement with the growth habit of the trigonal crystal. Furthermore, a local PFM study also showed the capability for non-180° polarization rotation (fig. S39). This means that a larger spontaneous polarization can be achieved in the corresponding polycrystalline sample after electric poling, facilitating the sample's practical applications in the thin-film form.

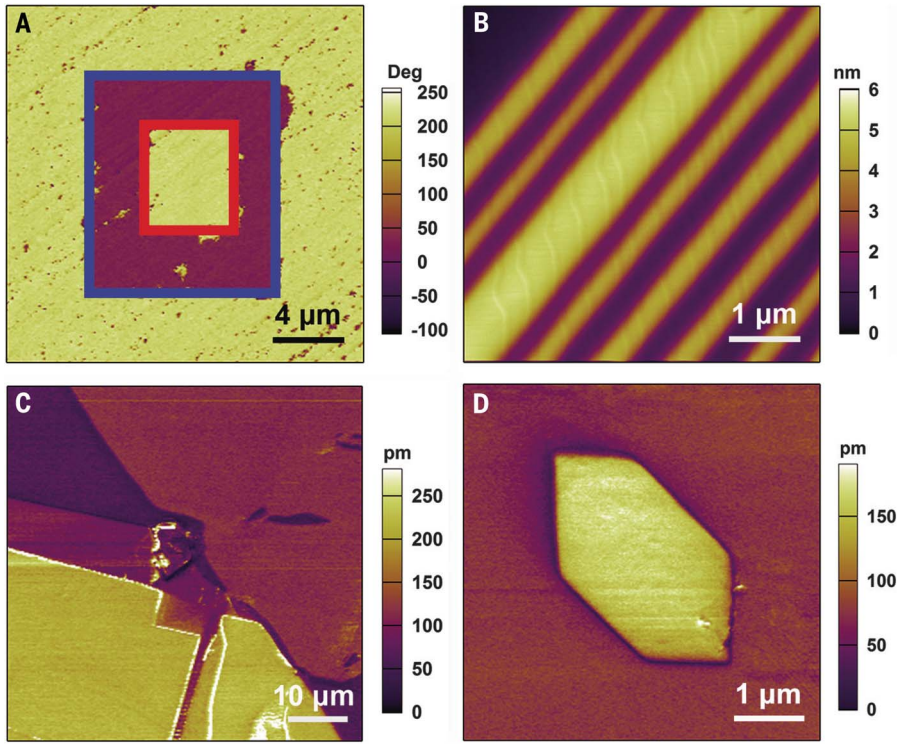

Fig. 3. PFM of MDABCO–NH_4I_3. (**A**) Out-of-plane PFM phase image recorded after writing an area of 10 μm by 10 μm with +100 V and then the central 5 μm by 5 μm square with −100 V by using a biased conductive tip in the bulk crystal. (**B** and **C**) PFM amplitude images in the as-grown microcrystals. (**D**) Out-of-plane PFM amplitude image after point polarization switching at the center point with positive bias at +40 V for 2 s in the microcrystal.

Other metal-free perovskite ferroelectrics

In addition to MDABCO–NH_4I_3, by changing the A cation and X anion according to the Goldschmidt tolerance factor, we have developed a wide variety of metal-free ABX_3-type 3D perovskite ferroelectrics (Fig. 4), such as ODABCO–NH_4Br_3 (ODABCO is *N*-hydroxy-*N*′-diazabicyclo[2.2.2]octonium) with an Aizu notation of 432*F*3, ODABCO–NH_4Cl_3 with $\bar{4}mFmm2$, *rac*-3AP–NH_4Br_3 (*rac*-3AP is *rac*-3-ammoniopyrrolidinium) with $m\bar{3}mFm$, *S*-3AQ–NH_4Br_3 (*S*-3AQ is *S*-3-ammonioquinuclidinium) with 432*F*2, and others (table S10). Chemical modifications of the constituent ions may promote the performance of the resulting ferroelectrics. For example, the spontaneous polarization will be enhanced by the introduction of ionic molecules with larger dipole moments. Moreover, using chiral template organic cations, we have successfully created optically active noncentrosymmetric organic perovskites. For example, molecular cationic isomers $(R\text{-3AP})^{2+}$ and $(S\text{-3AP})^{2+}$ and $(R\text{-3AQ})^{2+}$ and $(S\text{-3AQ})^{2+}$ can be easily embedded in ammonium halide cages because of their suitable geometric sizes and exact charge balancing. At room temperature, all these enantiomorphic perovskites crystallize in polar and chiral space group $P2_1$. The corresponding enantiomorphism relationships are verified both from single-crystal x-ray diffraction and vibrational circular dichroism (VCD) spectra (Fig. 4, C and D, and figs. S40 to S43). As expected, the infrared spectra of both enantiomorphic crystals are almost the same, whereas the corresponding VCD spectra are nearly mirror images. Hence, the introduction of organic components can lead to chemical diversity and chiral centers that may be impossible to achieve with inorganic perovskites. Homochiral molecules will form the enantiomorphic crystals of corresponding handedness that are easy to crystallize in the five enantiomorphic polar point groups (C_1, C_2, C_3, C_4, and C_6). Combining the high symmetry of 3D networks, this system can be regarded as an ideal target for the development of new multiaxial ferroelectrics, which hold great potential for use in thin-film devices because of their minimum requirements for crystallinity and specific substrates. Meanwhile, the optically active chiral compounds have a wide range of industrial and commercial applications, from uses in pharmaceutical and biological industries to applications as electro-optical elements (*49*, *50*), and ferroelectric optical activity may have a variety of potential applications.

Summary

We successfully designed a family of metal-free ABX_3-type 3D perovskites with high phase transition temperatures that are promising targets for new ferroelectric materials. In particular, MDABCO–NH_4I_3 has a large spontaneous polarization (P_s = 22 μC/cm^2) close to that of the

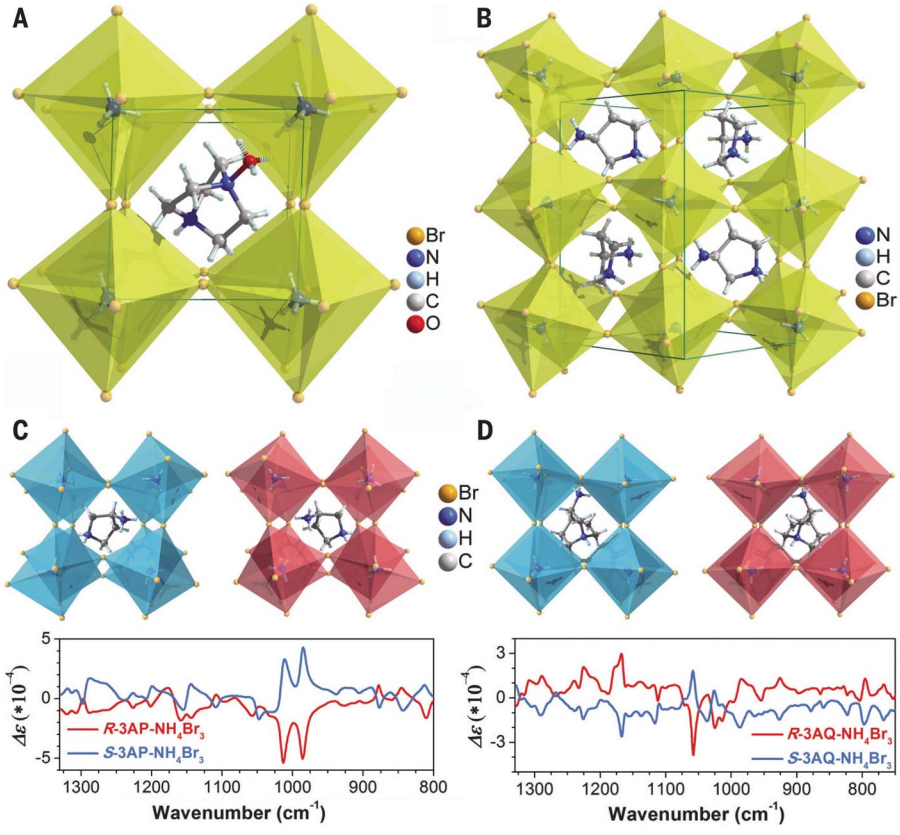

Fig. 4. Crystal structures and related chirality of the metal-free 3D perovskite ferroelectric family. Packing diagrams of (**A**) ODABCO–NH_4Br_3 and (**B**) *rac*-3AP–NH_4Br_3 in the ferroelectric phases. Crystal structures and measured VCD spectra of (**C**) *S*-3AP–NH_4Br_3 and *R*-3AP–NH_4Br_3 and (**D**) *S*-3AQ–NH_4Br_3 and *R*-3AQ–NH_4Br_3 in the ferroelectric phases. (Crystal structures of the analogs with Cl or I anions are shown in figs. S5 to S7.)

inorganic perovskite ferroelectric BTO (P_s = 26 μC/cm^2) and a high phase transition temperature (T_0 = 448 K) beyond that of BTO (390 K). The room-temperature processing not only reduces cost but also broadens the application potential by avoiding fracture during high-temperature annealing. Using PFM, we observed the coexistence of various ferroelectric domains with eight polarization directions, and we provided direct experimental proof that a flexible rotation of the polarization direction can occur in MDABCO–NH_4I_3 through the application of an electric field. The family of organic perovskites resembles inorganic perovskite ferroelectrics $PbTiO_3$, $BaTiO_3$, and $BiFeO_3$, as they can be optimized by using the Curie symmetry superposition principle and crystal engineering strategy. We believe that this class of materials, combining the outstanding ferroelectric properties and application advantages of molecular materials, holds great potential for the next generation of MEMS, flexible devices, wearable devices, and bionics.

REFERENCES AND NOTES

1. G. Rose, *Ann. Phys.* **124**, 551–573 (1839).
2. K. Hirose, R. Sinmyo, J. Hernlund, *Science* **358**, 734–738 (2017).
3. H. R. Wenk, A. Bulakh, *Minerals: Their Constitution and Origin* (Cambridge Univ. Press, 2016).
4. J. F. Scott, *Science* **315**, 954–959 (2007).
5. L. G. Tejuca, J. Fierro, *Properties and Applications of Perovskite-Type Oxides* (CRC Press, 2000).
6. L. Hu, S. Dalgleish, M. M. Matsushita, H. Yoshikawa, K. Awaga, *Nat. Commun.* **5**, 3279 (2014).
7. T. Akutagawa *et al.*, *Nat. Mater.* **8**, 342–347 (2009).
8. J. F. Scott, C. A. Paz de Araujo, *Science* **246**, 1400–1405 (1989).
9. M. E. Lines, A. M. Glass, *Principles and Applications of Ferroelectrics and Related Materials* (Clarendon Press, ed. 1, 1977).
10. F. Jona, G. Shirane, *Ferroelectric Crystals* (Pergamon, 1962), vol. 1.
11. S. Brittman, G. W. Adhyaksa, E. C. Garnett, *MRS Commun.* **5**, 7–26 (2015).
12. J. P. Correa-Baena *et al.*, *Science* **358**, 739–744 (2017).
13. Y. M. You *et al.*, *Science* **357**, 306–309 (2017).
14. N. Arora *et al.*, *Science* **358**, 768–771 (2017).
15. A. Kojima, K. Teshima, Y. Shirai, T. Miyasaka, *J. Am. Chem. Soc.* **131**, 6050–6051 (2009).
16. B. Saparov, D. B. Mitzi, *Chem. Rev.* **116**, 4558–4596 (2016).
17. J. Berry *et al.*, *Adv. Mater.* **27**, 5102–5112 (2015).
18. H. Cho *et al.*, *Science* **350**, 1222–1225 (2015).
19. Y.-H. Kim, H. Cho, T.-W. Lee, *Proc. Natl. Acad. Sci. U.S.A.* **113**, 11694–11702 (2016).
20. W. Li *et al.*, *Nat. Rev. Mater.* **2**, 16099 (2017).
21. W. J. Xu *et al.*, *J. Am. Chem. Soc.* **139**, 6369–6375 (2017).
22. Q. Pan *et al.*, *J. Am. Chem. Soc.* **139**, 3954–3957 (2017).
23. P. Jain, N. S. Dalal, B. H. Toby, H. W. Kroto, A. K. Cheetham, *J. Am. Chem. Soc.* **130**, 10450–10451 (2008).
24. P. Jain *et al.*, *J. Am. Chem. Soc.* **131**, 13625–13627 (2009).
25. D. W. Fu *et al.*, *Angew. Chem. Int. Ed.* **50**, 11947–11951 (2011).
26. C. A. Bremner, M. Simpson, W. T. A. Harrison, *J. Am. Chem. Soc.* **124**, 10960–10961 (2002).
27. L. A. Paton, W. T. Harrison, *Angew. Chem. Int. Ed.* **49**, 7684–7687 (2010).
28. Materials and methods are available as supplementary materials.
29. V. M. Goldschmidt, *Naturwissenschaften* **14**, 477–485 (1926).
30. G. Kieslich, S. Sun, A. K. Cheetham, *Chem. Sci.* **5**, 4712–4715 (2014).
31. K. Aizu, *J. Phys. Soc. Jpn.* **27**, 387–396 (1969).
32. D. Kleinman, *Phys. Rev.* **126**, 1977–1979 (1962).
33. C. B. Sawyer, C. Tower, *Phys. Rev.* **35**, 269–273 (1930).
34. S. Horiuchi, Y. Tokura, *Nat. Mater.* **7**, 357–366 (2008).
35. D. W. Fu *et al.*, *Science* **339**, 425–428 (2013).
36. H. L. Cai *et al.*, *Phys. Rev. Lett.* **107**, 147601 (2011).
37. R. E. Cohen, *Nature* **358**, 136–138 (1992).
38. R. Comes, M. Lambert, A. Guinier, *Solid State Commun.* **6**, 715–719 (1968).
39. W. Zhang, Y. Cai, R. G. Xiong, H. Yoshikawa, K. Awaga, *Angew. Chem. Int. Ed.* **49**, 6608–6610 (2010).
40. H. Y. Ye *et al.*, *J. Am. Chem. Soc.* **138**, 13175–13178 (2016).
41. P. F. Li *et al.*, *Nat. Commun.* **7**, 13635 (2016).
42. J. H. Lee, N. C. Bristowe, P. D. Bristowe, A. K. Cheetham, *Chem. Commun.* **51**, 6434–6437 (2015).
43. J. H. Lee, J. H. Lee, E. H. Kong, H. M. Jang, *Sci. Rep.* **6**, 21687 (2016).
44. G. A. Jeffrey, W. Saenger, *Hydrogen Bonding in Biological Structures* (Springer-Verlag, 1991).
45. D. Lee *et al.*, *Science* **349**, 1314–1317 (2015).
46. S. V. Kalinin *et al.*, *Annu. Rev. Mater. Res.* **37**, 189–238 (2007).
47. D. A. Bonnell, S. V. Kalinin, A. Kholkin, A. Gruverman, *MRS Bull.* **34**, 648–657 (2009).
48. V. Garcia *et al.*, *Nature* **460**, 81–84 (2009).
49. P. L. Polavarapu, *Chirality* **14**, 768–781 (2002).
50. M.-R. Goldsmith, N. Jayasuriya, D. N. Beratan, P. Wipf, *J. Am. Chem. Soc.* **125**, 15696–15697 (2003).

ACKNOWLEDGMENTS

We thank Y. Yan (University of Toledo) for help on DFT calculations. **Funding:** This work was supported by the 973 project (2014CB932103), the National Natural Science Foundation of China (91422301, 91622113, 21573041, 21574094, 21427801), and the Natural Science Foundation of Jiangsu Province (BK20150596 and BK20160029). **Author contributions:** H.-Y.Y. performed crystallographic analysis. Y.-Y.T. carried out the PFM study. P.-F.L., H.C., and P.-P.S. synthesized the sample. W.-Q.L. carried out ferroelectric characterization. J.-X.G. performed theoretical calculation. X.-N.H. carried out general characterizations. Y.-M.Y. and R.-G.X. conceived of the study and wrote the manuscript with input from other authors. **Competing interests:** All authors declare that they have no competing interests. **Data and materials availability:** All data are available in the main text or the supplementary materials.

SUPPLEMENTARY MATERIALS

www.sciencemag.org/content/361/6398/151/suppl/DC1
Materials and Methods
Supplementary Text
Figs. S1 to S43
Tables S1 to S12
References (*51–109*)

12 January 2018; accepted 6 June 2018
10.1126/science.aas9330

Metal-free three-dimensional perovskite ferroelectrics

Heng-Yun Ye, Yuan-Yuan Tang, Peng-Fei Li, Wei-Qiang Liao, Ji-Xing Gao, Xiu-Ni Hua, Hu Cai, Ping-Ping Shi, Yu-Meng You and Ren-Gen Xiong

Science **361** (6398), 151-155.
DOI: 10.1126/science.aas9330

Perovskites go organic

The perovskite structure accommodates many different combinations of elements, making it attractive for use in a wide variety of applications. Building perovskites out of only organic compounds is appealing because these materials tend to be flexible, fracture-resistant, and potentially easier to synthesize than their inorganic counterparts. Ye *et al.* describe a previously unknown family of all-organic perovskites, of which they synthesized 23 different family members (see the Perspective by Li and Ji). The compounds are attractive as ferroelectrics, including one compound with properties close to the well-known inorganic ferroelectric $BaTiO_3$.

Science, this issue p. 151; see also p. 132